Optical Absorption and Electron Spin Resonance in CuAlS$_2$:Ni

Igor AKSENOV, Tetsuya KAI, Nobuyuki NISHIKAWA and Katsuaki SATO

Faculty of Technology, Tokyo University of Agriculture and Technology, Koganei, Tokyo 184

Electron spin resonance (ESR) and optical absorption spectra have been studied in Ni-doped CuAlS$_2$ crystals, grown by the chemical vapour transport technique. Absorption spectra show optical transitions between 3d-shell originated orbitals of the Ni^{2+} ion, as well as charge-transfer transitions Ni^{3+}→Ni^{2+} and Ni^{2+}→Ni^{+}, their intensities being dependent on the position of the Fermi level in the bandgap of the host compound. The ESR results confirm the changes in the relative concentrations of Ni in different charged states caused by the Fermi level shift in the band gap, this shift, in its turn, being caused by thermal treatments of the crystals in various atmospheres.

1. Introduction

Ternary semiconductors of the type A^{1}B^{3}C$_2^6$ have been attracting much interest due to their promising luminescent and nonlinear optical properties. The CuAlS$_2$ compound is the widest band gap member of ternaries, which has recently been found to emit strong photoluminescence in the blue and green spectral regions[1] and, therefore, can be considered as a prospective material for blue and green LED application.

For technical application of CuAlS$_2$ it is necessary to understand the nature of the residual impurities incorporated in this compound, including that of transition atom (TA) impurities, which are known to introduce deep levels in the band gaps of semiconductors, including the ternary ones, these levels taking part in the processes of electrical charge compensation and acting as activators or killers of luminescence.[2] The optical properties of ternaries depend greatly on the charged state of the TA impurities, which, therefore, can be determined from optical measurements. Moreover, a defect whose energy is near the position of the Fermi level in the band gap will gain or lose electrons as the Fermi level passes through the demarcation level of different charged states of this defect. The position of the Fermi level can be influenced by appropriate thermal treatments of the host compound, and if any of the charged states of the defect are paramagnetic, the electron spin resonance (ESR) technique can be used to monitor the motion of the Fermi level in the vicinity of the demarcation level of the defect.

We have reported the observation of the internal d-d transitions in several TA ions of the iron group in CuAlS$_2$, i.e. V^{3+},[3] Mn^{2+}[4] and Co^{2+},[5] whereas charge-transfer transitions of the type TA^{3+}+e→TA^{2+} have been observed for Ti,[6] V,[3] Cr,[7] Fe[7,8] and Co[5] ions. The ESR results for TA impurities in the CuAlS$_2$ host have been reported for Ti^{3+},[6,9] V^{3+},[6] Cr^{+} and Mn^{2+},[7] Fe^{3+},[7,10] Fe^{2+},[11] Co^{2+}[12] and Ni^{+}.[13]

Although Ni is believed to be the third (after Fe and Cr) residual TA impurity in CuAlS$_2$,[7] the behaviour of this ion in the CuAlS$_2$ host lattice has not been studied in detail so far.

In this study we present the results of the ESR and optical absorption investigations of the CuAlS$_2$ crystals, doped with Ni.

2. Experimental

Single crystals of the CuAlS$_2$ compound doped with 0.2 mol% of Ni were grown by the temperature variation chemical vapour transport (CVT) technique in a closed system using iodine as a transporting agent.[5] The resulting Ni-doped crystals were typically plate-like ones with dimensions of about $0.5 \times 5 \times 5$ mm^3. Due to the very strong Ni-introduced absorption bands, discussed later, the crystals were opaque. Hence, for absorption measurements the crystals were mirror-polished to the thickness as small as 40 μm, the resulting polished samples exhibiting dark violet colouration in the transmitted light. Annealings of the Ni-doped crystals in vacuum, Cu or sulphur atmosphere were carried out for 60 h at 800°C with the pressure of S being ~5 atm.

Absorption spectra were measured at room temperature (RT) in the spectral range 400–2600 nm by using a Hitachi U-3410 spectrometer, as well as at 70 K, the samples in the latter case being put into an Oxford Instruments continuous flow cryostat. The low temperature measurements were carried out by using a halogen tungsten lamp as a light source and a JASCO CT-25C monochromator with the focal length of 25 cm as a disperser of the transmitted light. The dispersed light was then detected by a Hamamatsu R928 photomultiplier (in the range 400–900 nm), a North Coast Co. EO-817 Ge-detector (in the range 700–1800 nm), and an Infrared Associates Inc. InSb-detector (in the range 1400–2400 nm). All spectra were corrected for the spectral response of the detection system.

For ESR measurements relatively small bulk crystals were used, the ESR spectra being taken with a JEOL JES-RE2X X-band spectrometer at 110–130 K, the microwave power being 1–5 mW. The crystals used for ESR measurements were not oriented by X-ray techniques, but we were able to ascertain the approximate orientation of the crystals by checking the positions of the Fe^{3+}- and Ni^{+}-related signals.[7]

3. Results and Discussion

3.1 Optical absorption

The typical absorption spectra of undoped CuAlS$_2$ crystals have been found to exhibit two broad absorption bands peaked at 620 and 920 nm, causing the

green colouration of the crystals. These two bands originate from the charge-transfer transitions related to residual Fe^{3+} ions on Al-sites,[8] and at residual concentrations of the Fe impurity the contribution of these bands in the absorption coefficient is about 100 cm^{-1}.

Doping of the $CuAlS_2$ with Co causes drastic increase of absorption coefficient in the whole measured spectral region, the samples exhibiting two strong broad absorption bands C and D peaked at 1900 and 550 nm, respectively, a weaker A-band at 2200 nm, as well as a strong B-band, split into three components and centered at about 970 nm (Fig. 1, solid curve).

Having compared the general features of the spectrum shown by solid curve in Fig. 1 with that of the Ni-doped ZnS and CdS crystals,[14] we attributed the A- and B-bands to the internal d-d transitions in the divalent Ni ion, i.e. to the optically excited electronic transitions from the ground state of Ni^{2+} having $^3T_1$ symmetry to the excited states of $^3T_2$ (A-band) and $^3T_1$ (B-band) symmetry, split from the free ion F- and P-terms by the effect of the cubic component of the crystal field (Fig. 1, inset).

It should be noted that the observation of only two transitions (A- and B-bands, inset of Fig. 1) between 3d-shell-originated multiplets of the Ni^{2+} ion is not unexpected, since transitions from the ground state (spin=1) to the multiplets originated from ^1D free ion term (spin=0) are spin-forbidden, whereas transition from the ground state (essentially t^4e^4-configuration) to $^3A_2$ state (essentially t^2e^6-configuration) is of low probability because it involves a change of two electrons in the subshell configuration (two-electron jump).[15]

Now let us consider the fine structure of the B-absorption, which is shown in Fig. 2 and is believed to originate from the combined effect of the spin-orbit interaction and the noncubic (tetragonal) component of
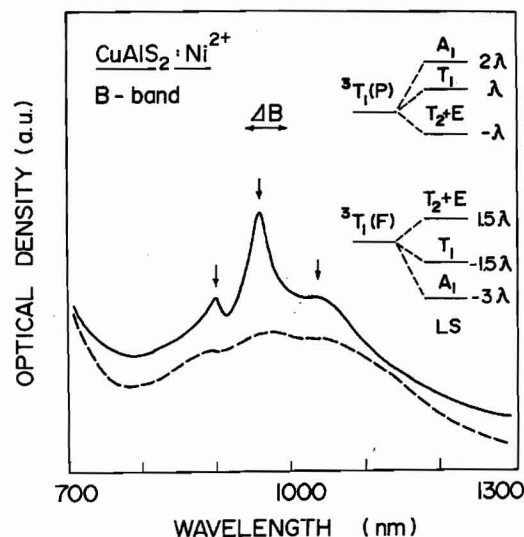
Fig. 2. Fine structure of the B-absorption band at RT (dashed curve) and 70 K (solid curve). In the inset the spin-orbit splitting of the B-band, expected from the crystal field theory, is shown.

the crystal field in the host lattice. We may expect the spin-orbit splitting of the levels for Ni^{2+} to be larger than that caused by the tetragonal component of the crystal field since 1) the spin-orbit constant for the free Ni^{2+} ion is quite large $(\lambda_0=340\ cm^{-1})^{14)}$ and 2) the noncubic component of the crystal field in $CuAlS_2$ is supposed to be quite small $(\sim200\ cm^{-1}$ for $CuGaS_2$,[16] which has the same ratio of the lattice periods $c/a=1.96$ as $CuAlS_2$).

The spin-orbit splitting of the levels, taking part in the B-absorption, is shown in the inset of Fig. 2.[14] It can be seen that in the first approximation the ground state is stabilized, due to the spin-orbit coupling effects, by the energy equals 3λ. Having adopted the value of λ for ZnS and CdS,[14] reduced due to the effect of covalency to $\lambda=250\ cm^{-1}$, and considering the spectral positions of the baricenters of the A- and B-absorption bands, we can estimate the values of the cubic crystal field parameter Dq and Racah parameter B as being equal to 475 and 460 cm^{-1}, respectively. The obtained value of Dq equals to that for Ni^{2+} in ZnS, whereas the value of B is smaller for $CuAlS_2$ than that for ZnS $(B=560\ cm^{-1})$,[14] which is an indication of a larger degree of covalency in $CuAlS_2$ as compared with ZnS.

The width ΔB of the B-band, expected from the spin-orbit splitting of the $^3T_1(F)$ and $^3T_1(P)$ states and taking into account selection rules,[14] is indicated above the spectra in Fig. 2 $(\Delta B \sim \lambda=250\ cm^{-1})$. It can be seen that the experimentally observed width of the B-band is much larger than ΔB. This discrepancy have been attributed to the effect of the noncubic component of the crystal field, which causes further splitting of all levels shown in the inset of Fig. 2 (except for the states of A_1 symmetry) and releases the selection rules. The configurational mixing of the $^3T_1(P)$ level with the levels originated from the upper ^1G and lower ^1D terms of the free Ni^{2+} ion may also contribute to the observed broadening of the B-band.
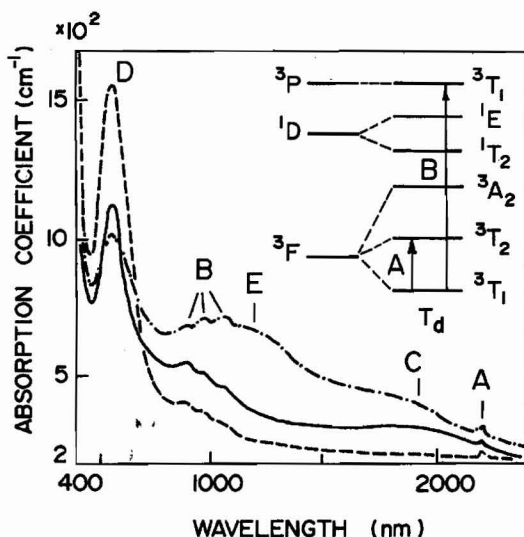

Fig. 1. Optical absorption spectra at RT of Ni-doped (solid curve), as well as subsequently vacuum-annealed (dashed curve) and S-annealed (dot-dashed curve) $CuAlS_2$ crystals. In the inset the splitting of the three lowest free ion terms of the Ni^{2+} ion in the cubic crystal field is shown.

Annealing experiments for the Ni-doped crystals show (returning to Fig. 1) that vacuum and Cu-annealings eliminate the C-band and, on the other hand, strengthen the D-band (Fig. 1, dashed curve), whereas annealing in S-vapour results in the opposite effect, i.e. in the strengthening of the C-band and diminishing the intensity of the D-band, as well as in the appearence of a broad strong E-absorption peaked at 1150 nm (Fig. 1, dash-dotted curve). Taking into account high intensity of the C- and D-bands, as well as the results for ZnS:Ni,[17] we have attributed the C- and D-bands to the $Ni^{3+} \rightarrow Ni^{2+}$ and $Ni^{2+} \rightarrow Ni^+$ charge-transfer transitions, respectively, whereas the E-band has been assigned to $Cr^{3+} \rightarrow Cr^{2+}$ charge-transfer transitions, the last assignment being based on our previous results.[7]

The relative intensities of the charge-transfer transitions between different charge (valence) states of TA ions are believed to be determined by the position of the Fermi level in the band gap of the host compound, which will be discussed in detail in §3.3.

Using the values of photoionization energies, corresponding to the spectral positions of the observed $Ni^{3+} \rightarrow Ni^{2+}$ and $Ni^{2+} \rightarrow Ni^+$ charge-transfer transitions, as well as the energy values for d-d transitions in Ni^{2+}, we have constructed a combined ionization and internal excitation diagram for Ni impurity in $CuAlS_2$ in comparison with that for ZnS,[17] which is shown in Fig. 3. A close resemblance of the observed behavior of Ni in $CuAlS_2$ and its binary analog ZnS is obvious.

The longer horizontal lines are demarcation levels, denoting ionization energies delineating the charge states $+/2+$ and $2+/3+$. The construct presented in Fig. 3 shows that Ni^{2+} oxidation state exists inside the band gap for both $CuAlS_2$ and ZnS hosts, whereas both Ni^+ and Ni^{3+} states are partly in resonance with the conduction band (CB) and the valence band (VB), respectively.

Following the approach of Zunger[17] we have assigned the ground state of Ni^{2+} to the Ni^{2+}/Ni^{3+} demarcation level. The said assignment, however, is consid-

ered as only an illustrational one since the ionization (demarcation) level is characteristic of two configurations (the Hartree-Fock approximation and Koopmans theorem are not valid for deep centers and, therefore, one ionization level is associated with two states) and, hence, the ionization level is not necessarily equatable with the ground state energy of one particular configuration (Ni^{2+} in our case).

3.2 ESR

The ESR spectra of the $CuAlS_2$ crystals, annealed in various atmospheres, are shown in Fig. 4. The observed ESR signals have been interpreted as follows:

●—a signal of Fe^{3+}, consisting of five fine structure transitions,[7] which are split into two components for perpendicular orientation of a magnetic field in relation to the c-axis of the crystals (Fig. 4(e)) due to the presence of two magnetically inequivalent metal sites in the chalcopyrite lattice,[18]

○—a highly anisotropic signal with $g_{//} \sim 8.5$, $g_\perp \rightarrow 0$, originating from transitions within the lowest non-Kramers doublet of Cr^{2+} ion,[6,7]

▼—an anisotropic signal with $g_\perp \sim 2g_{//} \sim 4.38$, which has been tentatively attributed to transitions within the $\pm 1/2$ Kramers doublet of Ni^{3+}, this assignment being based on the similar results for Ni^{3+} in the $CuGaS_2$ compound,[19]

■—a superposition of two ESR signals, i.e. a signal of Cr^+, consisting of five fine structure lines with

Fig. 4. ESR spectra of the $CuAlS_2$ crystals, doped with Ni, as well as subsequently annealed in various atmospheres. ●, ○, ▼, ■ and □ marks correspond to the signals from Fe^{3+}, Cr^{2+}, Ni^{3+}, $Cr^+ + Ni^+$ (two signals) ions and an unidentified impurity with a nearly isotropic $g \sim 11.95$, respectively.
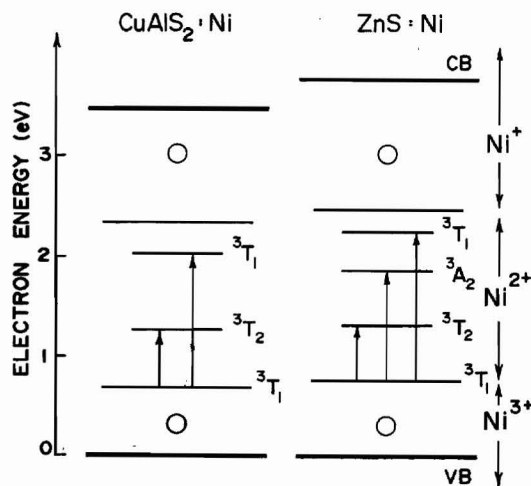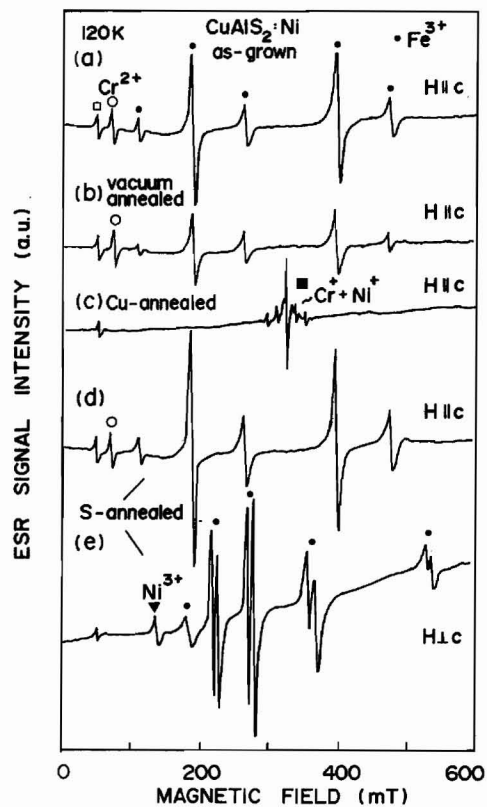

Fig. 3. A combined energy-level diagram showing d-d internal transitions and ionization levels of the Ni impurity in $CuAlS_2$ in comparison with that in ZnS. The states detected by ESR are marked by ○.

isotropic $g=1.998$,[7] and that of Ni^+, exhibiting one slightly anisotropic ($g_{//}=2.05$, $g_\perp=2.31$) transition within the lowest Kramers doublet, the observed anisotropy of the Ni^+ signal being caused by the spin-orbit mixing of the lowest doublet with the upper Kramers doublets,[13] and

□—a nearly isotropic signal at $g \sim 11.95$, originating from some unidentified impurity, the ground state of which carries a large amount of orbital momentum.[7] The last signal will not be considered in the following discussion.

The typical ESR spectrum of as-grown $CuAlS_2$:Ni crystals has been found to exhibit the Fe^{3+}- and Cr^{2+}-related signals, whereas annealings in oxidizing and reducing atmospheres results in strengthening or quenching of these signals, as well as in the appearence of signals from other paramagnetic centers (Fig. 4). The annealing-induced changes in the ESR spectra can be attributed to the Fermi level motion in the band gap of the host crystal, as discussed in the next section.

3.3 Effect of annealings-Fermi level motion

Now let us discuss the observed changes in the absorption (Fig. 1) and ESR (Fig. 4) spectra of $CuAlS_2$:Ni, introduced by annealing experiments. A schematic energy-level diagram for the three main TA impurities in $CuAlS_2$ (Fe, Cr and Ni) is shown in Fig. 5, where horizontal lines denote ionization energies (demarcation levels) of Fe, Cr and Ni impurities deduced from the spectral positions of the charge-transfer bands in the absorption spectra. Since we were not able to detect $Cr^{2+} \rightarrow Cr^+$ photoionization, the Cr^+/Cr^{2+} demarcation level is shown by the dashed line.

Now, using the Figs. 1, 4 and 5, let us consider the annealing-induced changes in the Fermi level position.

a) As-grown crystals

Since the as-grown $CuAlS_2$ crystals usually exhibit p-type conductivity with high resistivity values,[20] we believe that in the as-grown crystals the Fermi level is shifted down a little from the midgap position, the Fermi level being lower than $2+/3+$ demarcation level
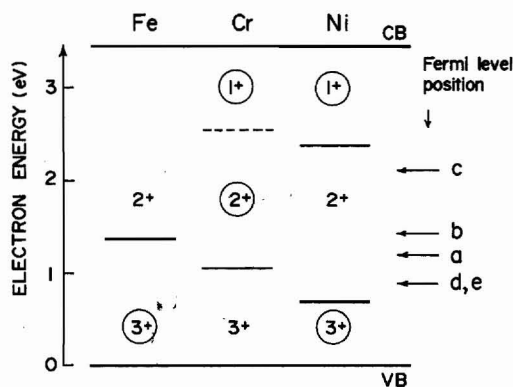
of Fe and higher than that of Cr and Ni. Therefore, most of Fe in as-grown crystals is present in the oxidation state Fe^{3+}, whereas the dominant oxidation states of Cr and Ni are Cr^{2+} and Ni^{2+}.

In the optical absorption spectra we observe the $Fe^{3+} \rightarrow Fe^{2+}$, $Cr^{3+} \rightarrow Cr^{2+}$ (in case of undoped crystals),[7] as well as $Ni^{3+} \rightarrow Ni^{2+}$ and $Ni^{2+} \rightarrow Ni^+$ photoionizations (Fig. 1). The intensity of the C-absorption band is smaller than that of the D-band since the relative concentration of Ni^{2+} as compared with Ni^+ (will be denoted as $Ni(2+/+)$) is higher than the relative concentration of Ni^{3+} in comparison with Ni^{2+} (will be denoted as $Ni(3+/2+)$). The ESR spectrum of as-grown crystals exhibits the signals from the dominant oxidation states of impurities—Fe^{3+} and Cr^{2+}. We could not detect the ESR signal of Ni^{2+}, probably because this ion ($3d^8$-configuration) is a non-Kramers ion.

b) Vacuum annealed samples

Annealing in vacuum leads to the increase in the concentration of the donor-like S-vacancies (V_S). This increase results in the upward shift of the Fermi level, this shift, in its turn, causing the increase in relative concentrations of Fe^{3+} as compared with Fe^{2+} and Cr^{3+} as compared with Cr^{2+} (will be denoted as $Fe(3+/2+)$ and $Cr(3+/2+)$). Experimentally we observe the decrease in the intensities of the ESR signal from Fe^{3+} without noticeable change in the intensity of Cr^{2+}-related signal.

As for Ni, the upward shift of the Fermi level results in the increase in the concentration of both Ni^+ and Ni^{2+}, and in the decrease in the concentration of Ni^{3+}. Therefore, 1) the relative concentration $Ni(3+/2+)$ decreases, which leads to the decrease in intensity of the C-absorption band, and 2) since the increase in the concentration of Ni^{2+} is larger than that of Ni^+, the relative concentration $Ni(2+/+)$ increases, which results in the increase of intensity of the D-absorption band.

c) Cu-annealed samples

Annealing in the presence of Cu results in the further upward shift of the Fermi level due to the increase in the concentration of V_S (donors) combined with the decrease in the concentration of V_{Cu} (acceptors) since Cu has been found to diffuse readily through the crystal lattice.[7]

In this case all iron exists in its divalent state, whereas Cr and Ni are partly converted into their monovalent states. In the ESR spectrum we observe, therefore, the complete quenching of the Fe^{3+}-related signal and an appearence of Ni^+- and Cr^+-originated signals, whereas the optical absorption spectrum does not change noticeably as compared with the vacuum annealed samples (not shown in Fig. 1).

d,e) S-annealed samples

Thermal treatment in S-vapour leads to the decrease in the concentration of the donor-like V_S defects, resulting in the downward shift of the Fermi level towards the valence band. In this case the concentrations $Fe(3+/2+)$ and $Cr(3+/2+)$ increase, the dominant oxidation states of Fe and Cr being turned into Fe^{3+} and Cr^{3+}. Therefore, we observe the strengthening of the Fe^{3+}-related ESR signal and the appearence of the

Fig. 5. A schematic energy-level diagram of $CuAlS_2$:Fe, Cr, Ni. The states detected by ESR are marked by ○. The position of the Fermi level in the band gap is indicated in the right part of the figure for; a: as-grown, b: vacuum annealed, c: Cu-annealed, and e, d: S-annealed samples. Note that the same indication is used in Fig. 4 to simplify the discussion.

strong $Cr^{3+} \rightarrow Cr^{2+}$ photoionization (E-band) in the absorption spectra.

Contrary to the case of vacuum annealing, annealing in sulphur leads to the increase of the concentration Ni(3+/2+) and to the decrease of the concentration Ni(2+/+), which results in the experimentally observed strengthening of the $Ni^{3+} \rightarrow Ni^{2+}$ absorption (C-band) and decrease in intensity of the $Ni^{2+} \rightarrow Ni^{+}$ absorption (D-band). Since Ni is now present in the Ni^{2+} and Ni^{3+} oxidation states, we observe quenching of the Ni^{+}-related signal and the appearence of Ni^{3+}-related signal in the ESR spectra.

4. Conclusions

In conclusion, we have shown in this paper that in as-grown CuAlS$_2$:Ni crystals the dominant oxidation states of Fe, Cr and Ni are, respectively, Fe^{3+}, Cr^{2+} and Ni^{2+}.

We have also shown that the oxidation states of TA impurity ions (Ni, Cr, Fe) and their relative concentrations in each oxidation state are controlled by the position of the Fermi level in the band gap of the host compound in relation to the demarcation levels of TA ions, denoting ionization energies delineating the charge states TA^{+}/TA^{2+} and TA^{2+}/TA^{3+}, the position of the Fermi level, in its turn, being dependent on the concentrations of the native donor- and acceptor-like defects, which can be controlled to the large extend by the proper thermal treatments of the crystals.

Acknowledgments

1) I. Aksenov and K. Sato: Appl. Phys. Lett. **61** (1992) 1063.
2) K. Sato, H. Tsunoda and T. Teranishi: *Proc. 7th Int. Conf. Ternary & Multinary Compounds, Snowmass, CO., 1986* (Mater. Res. Soc., Pittsburgh, 1987) p. 459.
3) I. Aksenov, Y. Kudo and K. Sato: Jpn. J. Appl. Phys. **31** (1992) L145.
4) K. Sato, M. Morita, S. Okamoto, S. Morita, T. Kambara, K. I. Gondaira and H. Takenoshita: Prog. Cryst. Growth Charact. **10** (1985) 311.
5) I. Aksenov, T. Kai, N. Nishikawa and K. Sato: Jpn. J. Appl. Phys. **32** (1993) L516.
6) I. Aksenov and K. Sato: Jpn. J. Appl. Phys. **31** (1992) L527.
7) I. Aksenov and K. Sato: Jpn. J. Appl. Phys. **31** (1992) 2352.
8) K. Kondo, T. Teranishi and K. Sato: J. Phys. Soc. Jpn. **36** (1974) 311.
9) U. Kaufmann, A. Räuber and J. Schneider: J. Phys. C **8** (1975) L381.
10) G. Brandt, A. Räuber and J. Schneider: Solid State Commun. **12** (1973) 481.
11) U. Kaufmann: Solid State Commun. **19** (1976) 213.
12) U. Kaufmann, A. Räuber and J. Schneider: Solid State Commun. **15** (1974) 1881.
13) U. Kaufmann: Phys. Rev. B **11** (1975) 2478.
14) H. A. Weakliem: J. Chem. Phys. **36** (1962) 2117.
15) R. Pappalardo and R. E. Dietz: Phys. Rev. **123** (1961) 1188.
16) K. Suzuki, T. Kambara, K. I. Gondaira, K. Sato, K. Kondo and T. Teranishi: J. Phys. Soc. Jpn. **39** (1975) 1310.
17) A. Zunger: Solid State Phys. **39** (1986) 318.
18) J. Schneider, A. Räuber and G. Brandt: J. Phys. Chem. Solids **34** (1973) 443.
19) H. J. von Bardeleben, C. Schwab and A. Goltzene: Phys. Lett. A **51** (1975) 460.
20) I. Aksenov, I. Gilakov, V. Lipnitskii, A. Lukomskii and L. Makovetskaya: Phys. Status Solidi a **115** (1989) K113.